Optimization of a smart structure to enhance the reliability and vibrations mitigation/harvesting performances

J. P. Sena, N. Kacem, A. M. G. de Lima, N. Bouhaddi

Abstract With the rise of research around smart materials, the use of shunted piezoceramics for dynamic vibration control has spread mostly because of its characteristics, for example capacity to absorb strain energy of a vibrating system and transform it into electrical energy. Since shunt/conversion circuit can both attenuate the vibrations amplitudes and harvest the energy dissipated, it becomes challenging to design and analyse the behaviour of the structure in such hybrid mitigation/harvesting conditions, taking into account reliability of this smart structure. This work aims to obtain the design parameters of the structure for compromise between maximum energy and minimum damage through a multiobjective optimization.

1 Introduction

For safety and economical reasons, the vibration control and monitoring of structures has great importance in the offshore, civil, mechanical and aeronautical engineering

João Pedro Sena
Federal University of Uberlândia, Department of Mechanics, Uberlândia, Brazil e-mail: joaopedrosena@ufu.br
University of Franche-Comté, FEMTO-ST Institute, Department of Applied Mechanics Besançon, France e-mail: joaopedro.sena@femto-st.fr

Najib Kacem
University of Franche-Comté, FEMTO-ST Institute, Department of Applied Mechanics Besançon, France e-mail: najib.kacem@univ-fcomte.fr

Antonio Marcos Gonçalves de Lima
Federal University of Uberlândia, Department of Mechanics, Uberlândia, Brazil e-mail: amglima@ufu.br

Noureddine Bouhaddi
University of Franche-Comté, FEMTO-ST Institute, Department of Applied Mechanics Besançon, France e-mail: noureddine.bouhaddi@univ-fcomte.fr

communities [1]. High cycle vibrations results in fatigue damage which can change the stiffness of the structure, leading to premature wear and product failure [2]. A great number of control techniques has been proposed to mitigate these vibrations in many engineering fields [3, 4].

Among these approaches, the the smart materials has been gaining research interest lately. The shunted piezoceramics has most widespread applications due to its characteristics [5], for example the capacity to absorb the strain energy of a vibrating system and transform it into electrical energy that can be used to drive electronic devices [6, 7]. As a result, vibrating energy harvesting (VEH) emerges as an alternative for small devices, particularly for aeronautical vehicles that require a limited amount of energy during operation [8].

Since the shunt/conversion circuit can both attenuate the vibrations amplitudes and harvest the energy dissipated, it becomes interesting to analyse the behaviour of the structure in such conditions, designing the structure and shunt/conversion circuit to harvest the maximum of energy while quantifying the increase of fatigue reliability of the whole smart structure. Many multiaxial fatigue damage criteria exist [9, 10, 11], but none of them is completely adapted to deal with predicting the fatigue reliability life of smart structures using piezoelectric shunt/conversion damping devices. Hence, the aim of this work is to develop a structural modelling of a vibration energy harvester device accounting the fatigue reliability of the smart structure by reducing the vibration with the shunt/conversion circuit.

2 Numerical model

The numerical model chosen for this work consists in a cantilever beam, with a patch of piezoceramic material in the base, connected to a shunt/conversion circuit with impedance $Z(\omega)$ according to Fig. 1. The finite element is from the serendipity family with 8 nodes, and the mechanical theory is the first-order shear deformation.

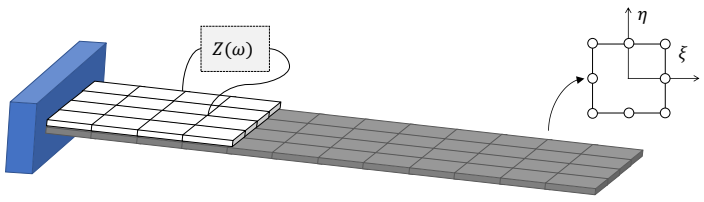

Fig. 1: Schematic of the structure and the shunt/conversion circuit.

Among the shunt/conversion circuits used with piezoelectric structures [15], it was considered in this work a resistive and a resonant circuit as shown in Fig. 2. The latter, composed by a resistance and an inductance in parallel, has the advantage of acting as a dynamic vibration absorber (DVA) [16] . The values of resistance

and inductance change the mechanical behaviour of the structure. These circuits are also known as monomodal circuits, since each tuning acts on a specific vibration frequency. The impedance $Z(\omega)$ of the resistive and resonant circuit is equal to R and $(Rj\omega L)/(R + j\omega L)$, respectively.

(a) Resistive (R) (b) Resonant in parallel (RL)

Fig. 2: Types of shunt/conversion circuits.

2.1 Eletromechanical Formulation

From the Hamilton's variational principle, the kinetic energy and the strain potential energy for a eletromechanical system are given, in the finite element method, as [12]:

$$E_c = \frac{1}{2}\int_{V_e} \rho \dot{\boldsymbol{U}}^T \dot{\boldsymbol{U}}\, \mathrm{d}V_e \qquad E_\varepsilon = \int_{V_e} \left(\boldsymbol{\varepsilon}^T \boldsymbol{\sigma} - \boldsymbol{E}^T \boldsymbol{D}\right) \mathrm{d}V_e \tag{1}$$

with $\boldsymbol{U}$ as the mechanical degrees of freedom, ρ the density of the element, V_e the volume of the element, $\boldsymbol{\varepsilon}$ the strain, $\boldsymbol{\sigma}$ the stress, $\boldsymbol{E}$ the electric field and $\boldsymbol{D}$ the electrical displacements. The electromechanical coupling of the system uses the material characteristics such as the mechanical properties $\boldsymbol{C}$, the dielectric constants $\boldsymbol{e}$ and the electric permittivity $\boldsymbol{\chi}$ to relate the stress and electrical displacement with the strain and electric field, respectivly:

$$\begin{Bmatrix} \boldsymbol{\sigma} \\ \boldsymbol{D} \end{Bmatrix} = \begin{bmatrix} \boldsymbol{C} & -\boldsymbol{e}^T \\ \boldsymbol{e} & \boldsymbol{\chi} \end{bmatrix} \begin{Bmatrix} \boldsymbol{\varepsilon} \\ \boldsymbol{E} \end{Bmatrix} \tag{2}$$

Considering the base of the multilayer finite element method and the kinetic energy, the matrix $\boldsymbol{N}$ containing the interpolation functions and the matrix $\boldsymbol{A}_u$ which contains the relation between the mechanical degrees of freedom and the displacement field are used to obtain the elementary mass matrix. In the theory of discrete equivalent layers [12], the mass and stiffness contribution of each layer is summed up to represent the element behaviour, up until the n-th layer. Similarly with the potential energy and the eletromechanical coupling, the matrices of material properties and the matrix $\boldsymbol{B}_{\{\bullet\}}$, which relates the interpolation functions with the strain field according to the linear elasticity theory, are used to obtain the stiffness matrices:

$$\begin{aligned} \boldsymbol{M}^{\{e\}} &= \sum_{k=1}^{n} \int_{V_k} \rho_k \boldsymbol{N}^T \boldsymbol{A}_u^T \boldsymbol{A}_u \boldsymbol{N} \, \mathrm{d}V_k \qquad & \boldsymbol{K}_{uu}^{\{e\}} &= \sum_{k=1}^{n} \int_{V_k} \boldsymbol{B}_u^T \boldsymbol{C} \boldsymbol{B}_u \, \mathrm{d}V_k \\ \boldsymbol{K}_{u\phi}^{\{e\}} &= \sum_{k=1}^{n} \int_{V_k} \boldsymbol{B}_u^T \boldsymbol{e} \boldsymbol{B}_\phi \, \mathrm{d}V_k & \boldsymbol{K}_{\phi\phi}^{\{e\}} &= \sum_{k=1}^{n} \int_{V_k} -\boldsymbol{B}_\phi^T \boldsymbol{\chi} \boldsymbol{B}_\phi \, \mathrm{d}V_k \end{aligned} \tag{3}$$

It is important to notice that the relation $\boldsymbol{K}_{u\phi} = \boldsymbol{K}_{\phi u}^T$ occurs by the characteristic symmetry. This elementary matrices are assembled following the classical connectivity methodology and result in a global mechanical dynamic system, with a displacement $\boldsymbol{u}(t)$, a potential energy $\boldsymbol{\phi}(t)$, an external force $\boldsymbol{f}(t)$, an electric charge $\boldsymbol{q}(t)$ [11] and with $\boldsymbol{C}_{eq} = \alpha \boldsymbol{M} + \beta \boldsymbol{K}_{uu}$ as the proportional Rayleigh's damping considered:

$$\begin{bmatrix} \boldsymbol{M} & 0 \\ 0 & 0 \end{bmatrix} \begin{Bmatrix} \ddot{\boldsymbol{u}}(t) \\ \ddot{\boldsymbol{\phi}}(t) \end{Bmatrix} + \begin{bmatrix} \boldsymbol{C_{eq}} & 0 \\ 0 & 0 \end{bmatrix} \begin{Bmatrix} \dot{\boldsymbol{u}}(t) \\ \dot{\boldsymbol{\phi}}(t) \end{Bmatrix} + \begin{bmatrix} \boldsymbol{K}_{uu} & \boldsymbol{K}_{u\phi} \\ \boldsymbol{K}_{\phi u} & \boldsymbol{K}_{\phi\phi} \end{bmatrix} \begin{Bmatrix} \boldsymbol{u}(t) \\ \boldsymbol{\phi}(t) \end{Bmatrix} = \begin{Bmatrix} \boldsymbol{f}(t) \\ \boldsymbol{q}(t) \end{Bmatrix} \tag{4}$$

The complex Frequency Response Function (FRF) can be obtained by assuming harmonic motion in the system, with $\boldsymbol{u}(t) = \boldsymbol{U}_0 \mathrm{e}^{j\omega t}$, $\boldsymbol{\phi}(t) = \boldsymbol{\Phi}_0 \mathrm{e}^{j\omega t}$, $\boldsymbol{f}(t) = \boldsymbol{F}_0 \mathrm{e}^{j\omega t}$ and $\boldsymbol{q}(t) = \boldsymbol{Q}_0 \mathrm{e}^{j\omega t}$. After some manipulations of the precedent equations, it is possible to obtain the following displacement FRF and voltage (potential) FRF:

$$\boldsymbol{H}_u(\omega) = \left[\boldsymbol{KCM} - \boldsymbol{K}_{u\phi} \left(\boldsymbol{K}_{\phi\phi} - \frac{1}{j\omega \boldsymbol{Z}} \right)^{-1} \boldsymbol{K}_{\phi u} \right]^{-1} \tag{5}$$

$$\boldsymbol{H}_\phi(\omega) = \left[\boldsymbol{K}_{\phi u} \boldsymbol{KCM}^{-1} \boldsymbol{K}_{u\phi} + \frac{1}{j\omega \boldsymbol{Z}} - \boldsymbol{K}_{\phi\phi} \right]^{-1} \boldsymbol{K}_{\phi u} \boldsymbol{KCM}^{-1} \tag{6}$$

For the sake of representation, the therm $\boldsymbol{KCM} = \left(\boldsymbol{K}_{uu} + j\omega \boldsymbol{C}_{eq} - \omega^2 \boldsymbol{M} \right)$ is used. The output power of the system is considered by calculating the power of the shunt/conversion circuit ($P = V^2/R$), and the average output power is calculated considering one vibration cycle of the frequency ω:

$$P_{av} = \frac{1}{2} \frac{\overline{H}_\phi^2}{R} \tag{7}$$

where $\overline{H}_\phi$ is the scalar voltage of the connection point in the piezoceramic layer. The Eq. 7 will be used in the multiobjective optimization process to enhance the harvested power.

2.2 Fatigue reliability

It is broadly assumed that the initiation of a crack in a structure under in-phase loads depends on the second invariant of the deviatoric stress tensor, but in non-proportional load, the activation of a greater number of slip bands may invalid this consideration [13]. Based in the work of [10], this multiaxial criteria aims to design engineering structures based on the endurance limit at 10^6 cycles or more. The Sines' criterion give good predictions, and considers the equivalent shear stress amplitude (square root of the second invariant amplitude) $\sqrt{J_{2,a}}$, the mean hydrostatic stress $\mathbb{E}\left[p_t(t)\right]$, the endurance limit for the torsion stress $\tau_{\text{-}1}$ and material constant ratio m [14]:

$$\sqrt{J_{2,a}} \leq f_{eq} = \tau_{\text{-}1} - (3m - \sqrt{3})\mathbb{E}\left[p_h(t)\right] \tag{8}$$

Having the vector $\boldsymbol{s}(t) = \left[s_{xx}(t)\ s_{yy}(t)\ s_{zz}(t)\ s_{xy}(t)\ s_{yz}(t)\ s_{xz}(t)\right]^T$ as the collect of the stress tensor and considering an in-phase loading from the alternating components, the square root of the second invariant can be determined according to the solid mechanics stress theory. The critical plane criteria are more appropriate when there's a fixation of the principal stress directions. Considering the second invariant of the deviatoric stress tensor in a five-dimensional Euclidean space E_5, and fixing each dimension as the semi-axes of the five dimension prismatic hull circumscribed to the loading path of the second invariant, the equivalent shear stress amplitude is calculated using Eq. 9 [10]. Considering a random state $\mathfrak{X}$ for the random equivalent shear stress amplitude, the deterministic second invariant is represented as $\sqrt{\mathfrak{J}_{2,a}}$.

$$\sqrt{J_{2,a}} = \sqrt{R_1^2 + R_2^2 + R_3^2 + R_4^2 + R_5^2} \xrightarrow{\mathfrak{x}} \sqrt{\mathfrak{J}_{2,a}} = \sqrt{\mathfrak{R}_1^2 + \mathfrak{R}_2^2 + \mathfrak{R}_3^2 + \mathfrak{R}_4^2 + \mathfrak{R}_5^2} \tag{9}$$

The results for the $\sqrt{\mathfrak{J}_{2,a}}$ are calculated based on the Gumbel distributions and were developped by [10]. Considering that the variables $\mathfrak{R}_i$ are not correlated:

$$\mathbb{E}\left[\left(\sqrt{\mathfrak{J}_{2,a}}\right)^2\right] = \sum_{i=1}^{5} \mathbb{E}\left[\mathfrak{R}_i^2\right] \qquad \mathbb{V}\left[\left(\sqrt{\mathfrak{J}_{2,a}}\right)^2\right] = \sum_{i=1}^{5} \mathbb{V}\left[\mathfrak{R}_i^2\right] \tag{10}$$

where, using the statistical moments definitions and Apery's constant $\zeta_3 \approx 1.20206$:

$$\mathbb{E}\left[\mathfrak{R}_i^2\right] = \mathbb{E}\left[\mathfrak{R}_i\right]^2 + \mathbb{V}\left[\mathfrak{R}_i\right] \tag{11}$$

$$\mathbb{V}\left[\mathfrak{R}_i^2\right] = 4\mathbb{E}\left[\mathfrak{R}_i\right]^2 \mathbb{V}\left[\mathfrak{R}_i^2\right] + \frac{22}{5}\mathbb{V}\left[\mathfrak{R}_i\right]^2 + 48\zeta_3\frac{\sqrt{6}}{\pi^3}\mathbb{E}\left[\mathfrak{R}_i\right]\mathbb{V}\left[\mathfrak{R}_i\right] - \mathbb{E}\left[\mathfrak{R}_i^2\right] \tag{12}$$

From the definition of the variance, $\mathbb{V}\left[\sqrt{\Im_{2,a}}\right] = \mathbb{E}\left[\left(\sqrt{\Im_{2,a}}\right)^2\right] - \mathbb{E}\left[\sqrt{\Im_{2,a}}\right]^2$. Knowing this, it is possible to write a non-linear equation involving $\mathbb{E}\left[\sqrt{\Im_{2,a}}\right]$ and this therms, which can be numerically solved using a Newton-Raphson methodology. Finally, the probability distribution of $\mathbb{E}\left[\sqrt{\Im_{2,a}}\right]$ is given by:

$$p_{\sqrt{\Im_{2,a}}}(r) = \frac{1}{\beta}\exp\left(-\frac{r-\mu}{\beta}\right)\exp\left(-\exp\left(-\frac{r-\mu}{\beta}\right)\right) \tag{13}$$

where the mode $\mu = \mathbb{E}\left[\sqrt{\Im_{2,a}}\right] - \beta\gamma$, the dispersion parameter $\beta = \frac{\sqrt{6}}{\pi}\left(\mathbb{V}\left[\sqrt{\Im_{2,a}}\right]\right)^{1/2}$ and $\gamma \approx 0.57721$ is the Euler-Mascheroni's constant. The Eq. 13 will be used as a mean damage indicator in the multiobjective optmization to minimize the strucutral damage.

3 Multiobjective optimization and results

The multiobjective optimization problem consists in the maximization of the average power defined by Eq. 7 and the minimization of the mean damage indicator defined by Eq. 13. The design variables of the shunt/conversion circuit parameters are R and L for the resonant circuit case and R for the resistive circuit case. The design variables of the structure are the thickness ratio δ_h and the length ration δ_l of the piezoelectric, both related to the respective parameter of the structure. The optimization problem can be defined as:

$$\begin{aligned} &\left\{\max f_1 = P_{av}\ ,\ \ \min f_2 = \mathbb{E}\left[\sqrt{\Im_{2,a}}\right]\right\}_{R,L,\delta_t,\delta_l} \\ &\quad s.t. \quad R_{min} < R \leq R_{max} \\ &\qquad\quad L_{min} < L \leq L_{max} \\ &\qquad\quad \delta_{min} < \delta_t, \delta_l \leq \delta_{max} \end{aligned}$$

To solve this multiobjective optimization problem, the well-known non dominated sorting genetic algorithm II (NSGA-II) was used.

The proposed simulation concerns a beam with length of 750 mm, width of 60 mm, thickness of 5 mm, made of an aluminium with $E = 70\,\text{GPa}$, $\nu = 0.33$, $\rho = 2700\,\text{kg/m}^3$, $R_m = 343\,\text{MPa}$ and $\tau_{-1} = 92\,\text{MPa}$. The bounds of the design variables are $[0, 1]\,\text{k}\Omega$ for the resistance R, $[0, 10]\,\text{H}$ for the inductance L and $[10\,\%, 40\,\%]$ for the ratios δ_t and δ_l. The optimal results located in the pareto's front are shown in Fig. 3. This figure illustrates the results of the resistive and the resonant cases. The points a and b represent the best compromise between harvested power and damage. The corresponding design variables are summarized in Table 1.

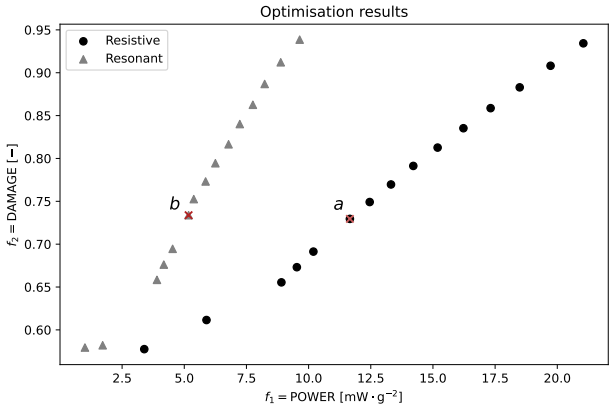

Fig. 3: Pareto's front.

Table 1: Optimal design variables (a: resistive case, b: resonant case)

Solutions	R	L	δ_t	δ_l	f_1	f_2
a	1000 Ω	–	0.35	0.30	12 mW · g^{-1}	0.73
b	622 Ω	10 H	0.37	0.30	5 mW · g^{-1}	0.73

For this specific modelled structure, the positions of fronts show that resistive circuit has the best compromise between the objectives. For the same value of damage, it produces a higher output power. One possible explanation for such a behaviour may be the main characteristic of resonant circuit, which attenuates vibrations by introducing an electrical resonance and acting as a mechanical absorber, opposed to resistive circuit.

4 Conclusion

In this work, a shunt/conversion circuit was designed accounting the agreement between output power and damage factor. The parameters of the circuit as well as the geometric dimensions of piezoelectric layer were defined as variables of the multiobjective optimization problem. Results show that, in this particular case, the resistive circuit has the best compromise. Further analysis may include a multimodal circuit configuration and more complex geometric considerations.

Acknowledgements

This study was financed in part by the Coordenação de Aperfeiçoamento de Pessoal de Nível Superior - Brasil (CAPES) – Finance Code 88887.696945/2022-00.

References

1. Montalvão D, Maia N M M, Ribeiro, A M R (2006) A Review of Vibration Based Structural Health Monitoring with Special Emphasis on Composite Materials. The Shock and Vib. Dig. 38:295–324
2. Friswell M I, Penny J E T, Wilson D A L (1994) Using vibration data statistical measures to locate damage in structures. The International J. of Analytical and Experimental Modal Analysis 9(4):239–254
3. Alkhatib R, Golnaraghi M F (2003) Active Structural Vibration Control: A Review. The Shock and Vib. Dig. 35(5):367–383, doi: 10.1177/05831024030355002
4. Balaji P S, Karthik SelvaKumar K (2020) Applications of Nonlinearity in Passive Vibration Control: A Review. J. Vib. Engineering & Technologies 9:183–213, doi: 10.1007/s42417-020-00216-3
5. Gripp J A B, Rade D A (2017) Vibration and noise control using shunted piezoelectric transducers: A review. Mechanical Systems and Signal Processing 112:359–383, doi: 10.1016/j.ymssp.2018.04.041
6. De Marqui Jr. C, Vieira W G R, Erturk A, Inman D J (2011) Modeling and analysis of piezoelectric energy harvestingfrom aeroelastic vibrations using the doublet-lattice method. J. of Vib. and Acoust. 133:1-–9
7. Erturk A, Inman D J (2011) Piezoelectric energy harvesting. 1ed, John Wiley & Sons Ltd, isbn: 978-0-470-68254-8
8. Li D, Wu Y, Ronch A R, Xiang J (2016) Energy harvesting by means of flow-induced vibrations on aerospace vehicles. Prog. in Aerosp. Sciences 86:28–62, doi: 10.1016/j.paerosci.2016.08.001
9. Pitoiset X, Preumont A (2000) Spectral methods for multiaxial random fatigue analysis of metallic structures. International J. of Fatigue 22(7):541–550, doi: 10.1016/S0142-1123(00)00038-4
10. Lambert S, Pagnacco E, Khalij A (2010) A probabilistic model for the fatigue reliability of structures under random loadings with phase shift effects. International J. of Fatigue 32:463-–474, doi: 10.1016/j.ijfatigue.2009.09.007
11. De Lima A M G, Lambert S, Rade D A, Pagnacco E, Khalij L (2014) Fatigue reliability analysis of viscoelastic structures subjected to random loads. Mechanical Systems and Signal Processing 43:305–318, doi: 10.1016/j.ymssp.2013.10.004
12. Faria A W (2006) Modelagem por elementos finitos de placas compostas dotadas de sensores e atuadores piezoelétricos: implementação computacional e avaliação numérica. Doctoral dissertation, Uberlândia, UFU
13. Doudard C, Calloch S, Cugy P, Galtier A, Hild F (2005) A probabilistic two-scale model for high-cycle fatigue life predictions. Fatigue Fract Eng Mater Struct 28(3):279–88
14. Papadopoulos IV, Davoli P, Gorla C, Filippini M, Bernasconi A (1997) A comparative study of multiaxial high-cycle fatigue criteria for metals. Int J Fatigue 19:219—35
15. Viana F A C (2005) Amortecimento de Vibrações usando Pastilhas Piezelétricas e Circuitos Shunt Ressonantes. Master dissertation, Uberlândia, UFU
16. Kim S M, Wang S, Brennan M J (2011) Dynamic analysis and optimal design of a passive and an active piezo-electrical dynamic vibration absorber. J. of Sound and Vib. 330(4):603–614, doi: 10.1016/j.jsv.2010.09.004